Connecting Mixing to Upwelling along the Ocean's Sloping Boundary

Alberto C. Naveira Garabato[1], Carl Pranas Spingys[2], Bieito Fernández Castro[1], Nicole Couto[3], Henri F Drake[4], Alexander Forryan[5], Zhiyuan Gao[6], Yuchen Ma[7], Herle Mercier[8], Marie-José Messias[9], Xiaozhou Ruan[10], Gunnar Voet[11], Bethan Lily Wynne-Cattanach[3], Raffaele Ferrari[12], Matthew H Alford[13], and Kurt Polzin[14]

[1]University of Southampton School of Ocean and Earth Science
[2]National Oceanography Centre
[3]Scripps Institution of Oceanography
[4]University of California Irvine
[5]University of Southampton
[6]Physical Oceanography Laboratory, Ocean University of China
[7]University of Cambridge
[8]French National Centre for Scientific Research (CNRS)
[9]University of Exeter
[10]Boston University
[11]Scripps Institution of Oceaonography
[12]Massachusetts Institute of Technology Department of Earth Atmospheric & Planetary Sciences
[13]University of California San Diego Scripps Institution of Oceanography
[14]Woods Hole Oceanographic Institution

September 12, 2025

Abstract

Deep-ocean upwelling, driven by small-scale turbulence, plays a key role in climate by regulating the ocean's capacity to sequester heat and carbon. Recent theoretical studies have hypothesized that such upwelling may primarily occur within a bottom boundary layer (BBL) along the sloping seafloor. A recent dye experiment in a continental-slope canyon as part of the BLT-Recipes program revealed very rapid BBL-focussed upwelling, endorsing this notion. Here, we elucidate the mixing processes governing the upwelling. We show that along-canyon upwelling stems from episodic turbulent mixing cells up to 250 m high, generated by tides sweeping up- and down-canyon. The tidal currents support a vertical shear that advects dense waters over slower-flowing lighter waters, reducing BBL stratification. This triggers instabilities that mix the dense waters with neighboring lighter waters, resulting in a net along-boundary upwelling flow. Our findings substantiate the view that deep-ocean upwelling can predominantly occur along the ocean's sloping boundaries.

Hosted file

GRL_BLT_mixing2upwelling.docx available at https://authorea.com/users/965505/articles/1334021-connecting-mixing-to-upwelling-along-the-ocean-s-sloping-boundary

Connecting Mixing to Upwelling along the Ocean's Sloping Boundary

Alberto C. Naveira Garabato[1], Carl P. Spingys[2], Bieito Fernández Castro[1], Nicole Couto[3], Henri F. Drake[4], Alexander Forryan[1], Zhiyuan Gao[1,5], Yuchen Ma[6], Herlé Mercier[7], Marie-José Messias[8], Xiaozhou Ruan[9], Gunnar Voet[3], Bethan L. Wynne-Cattanach[3], Raffaele Ferrari[6], Matthew H. Alford[3] and Kurt L. Polzin[10]

[1]Ocean and Earth Science, University of Southampton, Southampton, SO14 3ZH, UK.

[2]National Oceanography Centre, Southampton, SO14 3ZH, UK.

[3]Scripps Institution of Oceanography, University of California San Diego, La Jollxa, CA 92037, USA.

[4]Department of Earth System Science, University of California Irvine, Irvine, CA92697-3100, USA.

[5]Key Laboratory of Physical Oceanography, Ocean University of China, Qingdao, 266100, China

[6]Department of Earth, Atmospheric and Planetary Sciences, Massachusetts Institute of Technology, Cambridge, MA 02139, USA.

[7]Laboratoire de Physique des Océans, CNRS, UMR 6523 CNRS / Ifremer / IRD / UBO, Ifremer Centre de Brest, Plouzané, France.

[8]College of Life and Environmental Sciences, University of Exeter, Exeter, EX4 4QE, UK.

[9]Department of Earth and Environment, Boston University, Boston, MA 02215, USA.

[10]Woods Hole Oceanographic Institution, Woods Hole, MA 02543, USA.

Corresponding author: Alberto C. Naveira Garabato (acng@soton.ac.uk)

Key Points:

- The drivers of the rapid along-boundary upwelling observed by the BLT-Recipes dye experiment in a continental-slope canyon are investigated.
- It is shown that along-boundary upwelling stems from turbulent mixing cells up to 250 m high, generated by sheared tidal flows.

- The turbulence mixes the denser waters in the canyon with neighboring lighter waters, causing the dense waters to upwell along the boundary.

Abstract

Deep-ocean upwelling, driven by small-scale turbulence, plays a key role in climate by regulating the ocean's capacity to sequester heat and carbon. Recent theoretical studies have hypothesized that such upwelling may primarily occur within a bottom boundary layer (BBL) along the sloping seafloor. A recent dye experiment in a continental-slope canyon as part of the BLT-Recipes program revealed very rapid BBL-focussed upwelling, endorsing this notion. Here, we elucidate the mixing processes governing the upwelling. We show that along-canyon upwelling stems from episodic turbulent mixing cells up to 250 m high, generated by tides sweeping up- and down-canyon. The tidal currents support a vertical shear that advects dense waters over slower-flowing lighter waters, reducing BBL stratification. This triggers instabilities that mix the dense waters with neighboring lighter waters, resulting in a net along-boundary upwelling flow. Our findings substantiate the view that deep-ocean upwelling can predominantly occur along the ocean's sloping boundaries.

1 Introduction

Small-scale turbulent mixing has long been recognized as the key driver of deep-ocean diapycnal upwelling, through which dense abyssal waters of high-latitude origin are transformed into lighter, mid-depth waters (Munk, 1966; de Lavergne et al., 2016, 2021). Starting with Walter Munk's work in the 1960s, it has been extensively argued that upwelling is broadly distributed across the global ocean below ~1,000 m (Munk and Wunsch, 1998; Lumpkin and Speer, 2007; Talley, 2013), and that its underpinning mixing is induced principally by the breaking of internal waves radiating from rough topography (Munk and Wunsch, 1998; Kunze, 2017b; MacKinnon et al., 2017). A flaw in this argument is raised, however, by observations of the deep-ocean internal wavefield and associated turbulence: the intensity of such turbulence above rough topography – where the turbulence is commonly most vigorous – usually increases with depth (Waterhouse et al., 2014; Kunze et al., 2017a). This vertical structure of the turbulence implies that water parcels subject to wave breaking mix more rapidly with underlying denser layers than with overlying lighter waters, and so must become denser and

downwell – not upwell – across the ocean's density stratification (de Lavergne et al., 2016; Ferrari et al., 2016).

A potential solution to this conundrum is provided by a body of recent theoretical work (de Lavergne et al., 2016; Ferrari et al., 2016; Drake et al., 2020; Polzin and McDougall, 2021), founded on the principle that mixing must vanish at the ocean's solid boundaries. Since water parcels close to the seabed may only mix with overlying lighter waters, they must become lighter and *upwell* across stratification. If topography is sloped, as is often the case, such lightening of near-boundary waters could result in an upward along-boundary flow that would transport those waters to shallower depths. Thus, in this alternative view, deep-ocean diapycnal upwelling would expectedly occur via focussed and rapid along-boundary flows within an O(10 m)-thick, weakly stratified layer – the bottom boundary layer (BBL) – directed up sloping topography, with the downward reduction in mixing across the BBL governing the upwelling's intensity. Direct observational evidence in support of this scenario is lacking, however, so that the fundamental physics of BBL mixing and upwelling remain the focus of a vibrant discussion (Armi, 1979a,b; Garrett, 1979; Polzin and McDougall, 2021).

To address this evidence gap, the U.K.-U.S. Bottom Boundary Layer Turbulence and Abyssal Recipes (BLT-Recipes) program performed a suite of measurements of turbulent mixing, diapycnal upwelling and their driving processes along a paradigmatic ocean boundary: a continental-slope canyon, the likes of which occupy over one-fifth of all continental slopes bordering the global ocean (Harris and Whiteway, 2011; Harris et al., 2014). Measurements of the dispersion of a fluorescein dye injected near the seabed (Wynne-Cattanach et al., 2024) revealed the occurrence of exceptionally rapid diapycnal upwelling of O(10^{-3} m s^{-1}) [O(100 m d^{-1}), or roughly 10,000 times the global-mean deep-ocean upwelling rate (Munk, 1966; Munk and Wunsch, 1998; Lumpkin and Speer, 2007; Talley, 2013; de Lavergne et al., 2021)] along the canyon's thalweg. Here, we assess the mechanism by which turbulent mixing within the canyon results in such strong along-boundary upwelling.

2 Data and Methods

2.1 Data

The canyon targeted by BLT-Recipes is approximately 30 km long and 8 km wide at its entry, and is located in the Rockall Trough (Northeast Atlantic; Fig. 1a) – a basin characterized by generally moderate deep-ocean stratification and circulation (Holliday et al., 2015) and barotropic tidal currents (Stanev and Ricker, 2020). The observations considered here were obtained in July-October 2021, using both vessel-deployed and moored instrumentation. The ship-based measurements included (Fig. 1a): an along-canyon section of 11 full-depth hydrographic and (temperature and shear) microstructure profiles, which captures the general increase in the intensity of turbulence with proximity to the seabed (Fig. 1b) characteristic of regions of rough topography (Waterhouse et al., 2014; Kunze et al., 2017); 6 finely-resolved FastCTD (Klymak et al, 2006) timeseries of hydrographic and temperature microstructure profiles within the canyon spanning at least one semidiurnal tidal cycle (Alford et al., 2025); and the dye dispersion measurements (Wynne-Cattanach et al., 2024). The dye-derived diapycnal velocity of O(10^{-3} m s^{-1}) is equivalent to a warming of ~0.3°C d^{-1} as water parcels upwell across the canyon's stable background stratification, which is primarily determined by temperature (Fig. 1b; see also Suppl. Info.). High- (vertical and temporal) resolution records of turbulent fluctuations in three-dimensional velocity and temperature were acquired by a mooring instrumented with an acoustic Doppler current profiler (ADCP), 7 modular acoustic velocity meters and 83 thermistors, distributed across the deepest 300 m of the water column. The mooring was deployed near the canyon's head (Fig. 1a) for 89 days (i.e. ~172 semidiurnal and ~106 inertial periods), thereby affording robust statistical sampling of variability in turbulent parameters within the canyon across a broad range of frequencies (including tidal and near-inertial). See Suppl. Info. for further details.

2.2 Calculation of turbulent mixing rates from mooring-based temperature observations

To assess the evolution of mixing within the canyon, the rate of dissipation of temperature variance, χ, was computed from temperature timeseries acquired with each of the 83 fast-

sampling (1 Hz) thermistors in the mooring. χ is estimated from temperature records by fitting a theoretical model of inertial-subrange turbulence to measured temperature spectra (Shaw et al., 2001; Bluteau et al., 2013; Sreenivasan, 2018). See Suppl. Info. for a full model description. Implicit in the model are the assumptions of: Taylor's frozen field, used to relate horizontal wavenumber spectra to the measured frequency spectra (Shaw et al., 2001; Bluteau et al., 2013); a constant dissipation ratio, Γ, which relates the rate of turbulent kinetic energy dissipation, ε, to a buoyancy flux (Gregg et al., 2018); and a sole dependence of buoyancy frequency on temperature, found to accurately hold within the canyon. An estimate of χ was obtained for each thermistor every 5 minutes by, first, computing mean temperature spectra in 5-minute segments; and, second, fitting the theoretical model for periods of 10-100 s (or a suitably narrower range for near-bottom thermistors) representative of the inertial subrange. Γ was taken as 0.2 (as pertinent to much of the ocean; Gregg et al., 2018), but the sensitivity of χ to this choice was explored by repeating the calculation with Γ = 0.4 (likely more appropriate to our measured canyon; Alford et al., 2025). The calculation of χ from thermistor data entails several other practical computation choices, which introduce uncertainty. This uncertainty is discussed in the Suppl. Info., and found to be typically a factor of <2.

The mooring-based estimates of χ are of a subtly different nature to those acquired by the microstructure profilers – a distinction that has both advantages and challenges for our work. Profiler-based χ measurements are obtained at the closing stages of the turbulent cascade of temperature variance, i.e. near the dissipative (Kolmogorov) scale at which mixing takes place. Thus, they offer an accurate, relatively assumption-free view of local mixing. In contrast, mooring-based χ values are derived from observations within the inertial subrange, such that the measured temperature variance is yet to cascade further downscale before reaching the dissipative scale. A simple estimate of the timescale of the downscale cascade ($\langle T'^2 \rangle/\chi$, where $\langle T'^2 \rangle$ is the characteristic thermistor-measured potential temperature (T) variance on inertial-subrange timescales) suggests that it may take several hours for that variance to be dissipated. Consequently, mooring-based χ values provide an assumption-heavier, but spatially-integrated metric of the in-canyon mixing. The integral character of mooring-based χ estimates is arguably advantageous to our goal of connecting upwelling to mixing rates, as it reduces the sensitivity

of the calculation to the precise location of the mooring – which effectively samples mixing conditions along a substantial segment of the canyon. Since the in-canyon flow is highly rectilinear (oriented along-canyon) and varies primarily on semidiurnal tidal timescales, the along-canyon advective lengthscale corresponding to $\langle T'^2 \rangle / \chi$ may be estimated as O(100-1000 m), given a characteristic along-canyon tidal velocity of ~0.1 m s^{-1} (Fig. 1a).

A further advantage of mooring measurements is that they are approximately Eulerian, and thereby provide unbiased sampling of all phases of the tidal cycle. Whereas the mooring's uppermost instruments move horizontally by only <50 m during one such cycle, microstructure profilers may drift with the tidal currents by as much as ~3 km in the course of a cast (Alford et al., 2025). This drift is expected to curtail the extent to which profilers may sample the most vigorous mixing in a tidal cycle, which – as will be seen – takes place immediately below the strongest up-canyon flows. As a profiler descends into these intense flows, it will tend to be advected away from the highly-turbulent layers below, potentially introducing a sampling bias. This likely explains why Alford et al. (2025) did not observe buoyancy flux profiles consistent with upwelling.

2.3 Calculation of diapycnal upwelling from mooring-based temperature observations

The rate of diapycnal (closely equivalent to diathermal) upwelling, w_T^*, across the canyon's mean stratification is computed from the mooring-based estimates of χ. An expression for w_T^* may be derived by considering the diathermal flux (Winters and D'Asaro, 1996),

$$\phi = -\kappa \frac{\partial z^*}{\partial T} \langle |\nabla T|^2 \rangle_{z^*} , \qquad (1)$$

where z^* is the distance in the diathermal direction and $\langle \rangle_{z^*}$ denotes an average over a temperature surface in a bounded volume. Combining equation (1) with the definition of $\chi = 2\kappa \langle |\nabla T|^2 \rangle$ (where the angled brackets indicate an average over a local volume, with spatial

scales comparable to those of three-dimensional turbulence; Oakey, 1982) and expressing w_T^* as the rate of change of the diathermal flux in the diathermal direction yields:

$$w_T^* = -\frac{\partial \phi}{\partial z^*} = \frac{1}{2}\frac{\partial(\langle\chi\rangle_{z^*}\frac{\partial z^*}{\partial T})}{\partial z^*} = \frac{1}{2}\frac{\partial\langle\chi\rangle_{z^*}}{\partial T} + \frac{1}{2}\langle\chi\rangle_{z^*}\frac{\partial^2 z^*/\partial T^2}{\partial z^*/\partial T}. \qquad (2)$$

w_T^* has units of °C s^{-1}. Its definition synthesises the notion that a water parcel mixing with warmer waters more strongly than with colder waters will become warmer, or – since warm waters overlie cold waters in a stably-stratified column – will *upwell* across isotherms. Conversely, a water parcel mixing with colder waters more intensely than with warmer waters will become colder, or *downwell* across isotherms. Note that, since isopycnal gradients of temperature are negligible within the canyon, the in-canyon temperature variance is overwhelmingly produced by diapycnal flows, such that w_T^* is an accurate metric of the diapycnal velocity. w_T^* can be expressed in the more familiar units of m s^{-1} via scaling with the diathermal (close to vertical within the canyon) gradient of potential temperature, i.e. $w^* \approx w_T^* / \frac{\partial T}{\partial z*}$.

Our calculation of w_T^* from mooring-based estimates of χ makes two inevitable assumptions. First, z^* is approximated by the local vertical direction, i.e. the only direction sampled by the mooring. This approximation is supported by a comparison of directly-measured vertical temperature gradients with indirectly-estimated along-canyon temperature gradients (inferred via application of Taylor's frozen field). This comparison suggests that the characteristic magnitude of vertical gradients typically exceeds that of horizontal gradients by at least one order of magnitude on a wide range of timescales longer than those of the inertial subrange (i.e. ≫1 min), such that the diathermal direction is close to vertical on those timescales.

Second, $\langle\chi\rangle_{z^*}$, the isothermal average of χ within the bounded calculation volume, is assumed to be adequately represented by χ as sampled by the mooring at a specific tidal phase. Thus, tidal phase-averaged fields of χ and other relevant variables are constructed prior to

computation of w_T^*, and the $\langle\ \rangle_{z^*}$ operator is approximated by a tidal phase-average (see Suppl. Info. for details). There is no *a priori* justification for this approximation; rather, its adoption places subtle constraints on the interpretation of our w_T^* diagnostics. The 'bounded volume' to which these diagnostics apply may be regarded as a body of water centred at the mooring site, extending up to ~6 km (double the along-canyon semidiurnal tidal excursion) along the thalweg, and sloshing up- and down-canyon by up to ~3 km. Since the semidiurnal tidal cycle of χ exhibits the same characteristic patterns at different locations along the canyon (cf. Figs. 2c and S3d), our estimated w_T^* at any tidal phase can be thought of as the upwelling rate experienced by the volume at that phase. This would be the case even if different parts of the volume were subject to different tidal phases at any instant in time.

The calculation of w_T^* is performed in four steps. First, a vertical profile of χ is constructed at 5-minute intervals by bin-averaging all the χ estimates from individual thermistors within a half-bin period of each time-bin centre. Second, each vertical profile of χ is re-mapped onto temperature space by bin-averaging in temperature cells at intervals of 0.1°C. Third, phase averages of χ and z^* (approximated by the vertical coordinate) are computed. Fourth, $\partial\chi/\partial T$, $\partial z^*/\partial T$ and $\partial^2 z^*/\partial T^2$ are calculated in each time-bin and temperature class via centred differences. This step assumes that a single vertical mooring captures the bulk of the temperature dependence of χ. The resulting estimate of w_T^* is primarily determined by the $\frac{1}{2}\frac{\partial\langle\chi\rangle_{z^*}}{\partial T}$ term, although the contribution from the $\frac{1}{2}\langle\chi\rangle_{z^*}\frac{\partial^2 z^*/\partial T^2}{\partial z^*/\partial T}$ term is also significant and reinforces the patterns in the dominant term (Fig. S6). The uncertainty in w_T^* related to temporal variability and instrumental noise is assessed in the Suppl. Info., and displayed in Figure 3d.

3 Results

A window into the nature of the in-canyon turbulence is provided by the vessel-based timeseries of hydrographic and temperature microstructure profiles, an example of which is shown in Figures 2b,c contextualised with the mooring-measured along-canyon flow (Fig. 2a). The canyon's background hydrographic structure entails a reduction in temperature with depth

of ~1°C over 400 m (Fig. 2b), which corresponds to a buoyancy frequency of ~2×10^{-3} s^{-1} characteristic of deep-ocean stratification elsewhere (de Lavergne et al., 2016, 2021). This background structure is prominently modulated by a semidiurnal tide, which flows up- and down-canyon with peak speeds of ~0.2 m s^{-1} (cf. Figs. 2a,b). As the flood tidal flow displaces isotherms upward, a layer containing frequent patches of unstable stratification (within which temperature typically increases slightly with height above bottom; Fig. 2d) develops over 2-3 hours, reaching a height of ~250 m at the tide's turning. Vigorous mixing ($\chi > 10^{-8}$ $°C^2$ s^{-1}, exceeding typical ocean-interior values by over one order of magnitude) occurs along the turbulent layer's rising edge (Fig. 2c), a pattern suggestive of a convective mixing scenario in which isotherms fold over to produce areas of local static instability that progressively mix the fluid from above (Thorpe, 2005; Umlauf and Burchard, 2011; Ivey et al., 2021). During the ebb tide, isotherms deepen, the turbulent layer thins rapidly, the near-bottom water column re-stratifies, and elevated mixing is progressively confined closer to the seabed.

Strong shears can induce turbulent mixing of dense and light waters in the stably-stratified ocean interior through two primary mechanisms. First, a sufficiently strong and persistent shear can advect dense waters over lighter waters, inducing a convective instability (Moum et al., 2004; Umlauf and Burchard, 2011; Winters, 2015; Lorke et al., 2005, 2008). Second, weaker or less persistent shear can still be energetic enough to trigger a Kelvin-Helmholtz shear instability (Smyth and Moum, 2012; Lewin and Caulfield, 2022; Liu et al., 2023). This is typically assumed to occur when the Richardson number – the ratio of stratification to shear squared – is less than ¼, although for time-dependent shears, as is the case for the tidal flow here, the instability can occur at somewhat higher Richardson numbers (e.g., Si et al., 2025). Convective instabilities generate patches of turbulence with the same vertical scale of the sheared flow, while shear instabilities are typically more ephemeral and result in turbulent patches of O(1-10 m) and O(1-10 min).

The along-canyon tidal flow exhibits significant vertical shear (i.e. the tide is baroclinic; Fig. 2a), with flood and ebb tidal speeds usually peaking at >0.15 m s^{-1} about 250 m above the seabed

and decreasing to <0.05 m s^{-1} within ~50 m of the bottom. As this vertically-sheared flow advects the background temperature distribution – which consists of roughly flat isotherms (Fig. 1b) – along the canyon's sloping thalweg, it transports colder waters from further down the canyon over the slowly-moving near-bottom waters during periods of positive shear (upward-increasing up-canyon flow; e.g., during flood), causing unstable stratification and turbulent mixing about 3-6 h into that tidal phase (Figs. 2a,b). Conversely, this vertically-sheared flow carries warm waters from higher up the canyon over near-bottom waters during periods of negative shear (downward-increasing up-canyon flow; e.g., during ebb), acting to restore stably-stratified conditions (Figs. 2a,b). Thus, the occurrence of turbulent mixing and subsequent re-stratification can both be attributed to the differential advection of the canyon's background hydrographic structure by a vertically-sheared tide steered by the sloping topography. It remains somewhat unclear whether the shear is sufficiently strong and persistent to drive a convective instability, as argued by Alford et al. (2025), or whether turbulence results from a parametric shear instability, as proposed by Si et al. (2025). Both instabilities produce patches of unstable stratification and mixing across the vertical range of enhanced tidal shear, as observed. See further discussion in the Suppl. Info.

The role of turbulent mixing in driving the rapid diapycnal upwelling observed in the canyon (Wynne-Cattanach et al., 2024) may be quantitatively borne out by considering the mooring-based measurements, which – on account of their long extent (89 days) and high temporal resolution (~1 s) – capture the variability of mixing (assessed via χ; section 2.2) over many tidal cycles. The same semidiurnal sequence of isotherm shoaling and deepening, de- and re-stratification, and enhancement and suppression of χ, seen in the vessel-based observations (Fig. 2) is apparent in the mooring records (Fig. S3 and Supp. Movie), which also expose some differences between any two tidal cycles. To draw statistically robust relationships between mixing and its tidal drivers, and elucidate implications for upwelling, we construct a phase-averaged picture of the temporal evolution of the along-canyon flow (Fig. 3a) and χ (Fig. 3b) over a semidiurnal tidal cycle (see Suppl. Info.). Using T as the vertical coordinate provides a

ready connection between χ and the diathermal (here equivalent to diapycnal) velocity, w_T^*, expressed as a warming rate and defined by equation (2).

The phased-averaged view (Fig. 3c) demonstrates how, in a characteristic tidal cycle, isobaths progressively converge in temperature space (denoting de-stratification; Fig. 3a) and χ is elevated across a wide range of temperatures (Fig. 3b) when the flow ~200 m above the seabed is directed up-canyon relative to the near-bottom flow, i.e. precisely when positive shear peaks and stratification is minimal. This occurs at the tide's turning from ebb to flood (around a phase of 2 rad, when the flows far above and near the seabed are oriented oppositely) and during flood (in the phase range of 2.5-5 rad, when flow is up-canyon at all temperatures). The causal relationship between positive shear and χ also transpires in the latter's diathermal distribution: χ peaks along the band of maximum up-canyon shear, some ~120 m above the seabed (Fig. 3b; see also Fig. S5g), and decays toward colder temperatures from there, since the intensity of up-canyon flow varies little over the coldest waters, i.e. in the deepest ~80 m. Subsequently, as the tide turns to ebb (in the phase ranges of 0-1.5 rad and >5 rad), isobath divergence and a reduction in χ lead to re-stratification and suppression of turbulence.

The diapycnal circulation induced by the in-canyon turbulent mixing is illustrated by the phase-averaged distribution of w_T^* (Fig. 3c). During flood, the preferential elevation of χ within intermediate temperature classes (around 5°C; Fig. 3b) results in diapycnal upwelling (i.e. warming) of colder waters (typically within ~120 m of the seabed) at rates approaching or exceeding 10^{-5} °C s^{-1}, and in somewhat less intense diapycnal downwelling (i.e. cooling) of warmer waters aloft. Little diapycnal flow occurs during ebb. Upon averaging over the tidal cycle to estimate the net diapycnal velocity profile (Fig. 3d), waters colder than ~5°C are found to upwell at a rate of up to ~3×10^{-6} °C s^{-1} (~0.3 °C d^{-1}), and warmer waters to downwell at a weaker rate of ~-1×10^{-6} °C s^{-1} (~-0.1 °C d^{-1}), resulting in convergence and net formation of waters of intermediate temperatures (around ~5°C). The net upwelling rate of the colder waters approximately matches the dye-derived diapycnal flow of ~0.3 °C d^{-1} (Wynne-Cattanach

et al., 2024) – thereby endorsing the role of tidal shear-generated mixing in driving the rapid along-boundary upwelling measured within the canyon.

The efficacy of tidal shear-generated turbulence as an agent of intense diapycnal upwelling is contingent on its large vertical scale, which leads to the swift mixing of waters spanning a substantial range of temperatures. In our measured canyon, where turbulence is observed to reach up to ~250 m above bottom, such vertical scale is determined by that of the along-canyon flow's vertical shear – as it is this shear that reduces stratification by differentially advecting the background temperature profile along the canyon's sloping thalweg (Fig. S1). Our analysis (see Suppl. Info. and Fig. S4) suggests that the in-canyon vertical shear is associated with baroclinic tidal waves that develop within the canyon (Baines, 1983; Grimshaw et al., 1985; Ma et al., 2025). The characteristic vertical scale of the waves is on the order of the canyon's vertical extent, which thus sets the size of the large turbulent overturns underpinning along-slope upwelling.

4 Conclusions

In conclusion, our observations of a continental-slope canyon at the edge of a North Atlantic basin provide evidence of very rapid along-boundary upwelling driven by vertically-extensive turbulent mixing, itself generated by semidiurnal baroclinic tidal flows sloshing up- and down-canyon (Fig. 4). The cornerstone of the upwelling mechanism is the sheared structure of the tidal waves that develop within the canyon. When steered by the canyon's sloping thalweg, this shear advects dense waters above lighter near-bottom waters during flood, thereby reducing stratification and priming the BBL for convective and shear instabilities. These instabilities produce overturns that mix dense BBL waters with surrounding lighter waters (Fig. 4a), resulting in diapycnal upwelling along the canyon. Reversal of the sheared tidal flow during ebb induces re-stratification within the canyon via the differential down-canyon advection of near-boundary waters (Fig. 4b), and promotes the offshore export of waters that were newly mixed and upwelled along topography during the previous flood (Wynne-Cattanach et al., 2024). Such ebb-time re-stratification and export reset the canyon for the next flood stage of

upwelling, and communicate the effects of in-canyon mixing and upwelling toward the basin's interior.

Although the technological complexity of our measurements inevitably confines our study to a single small domain, there is evidence to suggest that our findings may have wider representativeness along other sloping boundaries. Such evidence comes in two forms. First, canyons of a similar nature to that of the one targeted here abound around the global continental slope. Our measured canyon's length (~30 km), width (~8 km at its mouth), vertical extent (>1000 m from mouth to head), aspect ratio (~80º, denoting a relatively narrow canyon), V-shaped geometry (with axial slope near M2 tidal criticality, and steep, supercritical sidewalls), and characteristic barotropic tidal speeds (~0.08 m s^{-1}) – all factors likely to shape the governing physics and intensity of the in-canyon mixing (Nazarian and Legg, 2017a,b) – are in line with those of many continental-slope canyons in the global ocean (Harris and Whiteway, 2011; Harris et al., 2014; Nazarian et al., 2021). The degree of criticality of the thalweg is likely to be particularly important in generating the strong near-bottom baroclinic flows required to support mixing as vigorous as that in our measured canyon (Slinn and Riley, 1996; Nazarian and Legg, 2017a,b; Nazarian et al., 2021; Ma et al., 2025). Second, observational and modelling investigations of near-boundary mixing in a range of oceanic (Moum et al., 2004; Umlauf and Burchard, 2011; Winters, 2015; Schulz and Umlauf, 2016; Baker et al., 2023; Masunaga et al 2025), limnic (Lorke et al., 2005, 2008) and idealized geophysical fluid (Lewin and Caulfield, 2022; Liu et al., 2023; Si et al., 2025) settings suggest that the shear-driven destabilization process documented here may be of some generality to oscillatory flows over sloping topography, regardless of the details of the flow or topographic configuration. On this basis, our results provide observational support for the paradigm of BBL-focussed deep-ocean upwelling, and point to shear-generated instabilities as a potentially important agent of such upwelling.

Acknowledgments

The BLT programme is supported by the U.S. National Science Foundation (grant OCE-1756264, OCE-1756324) and the U.K. Natural Environment Research Council (grant NE/S001433/1). We are grateful to the scientific party, crew and technicians on the *RRS Discovery* for their hard

work during data collection; and to Sjoerd Groeskamp and Hans van Haren for their insightful feedback on the manuscript.

Open Research

The microstructure data are publicly available at https://doi.org/10.17882/98178. The mooring data are publicly available at https://doi.org/10.5061/dryad.v15dv424f. The multi-beam bathymetry data are publicly available at https://doi.org/10.17882/99872.

References

Alford, M. H. *et al.* Buoyancy flux and mixing efficiency from direct, near-bottom turbulence measurements in a submarine canyon. *J. Phys. Oceanogr.*, **55**, doi:10.1175/jpo-d-24-0005-1 (2025).

Armi, L. Some evidence for boundary mixing in the deep ocean. *J. Geophys. Res.* **83**, 1971-1979 (1979).

Armi, L. Reply to comments by C. Garrett. *J. Geophys. Res.* **84**, 5097-5098 (1979).

Baines, P. G. Tidal motion in submarine canyons – A laboratory experiment. *J. Phys. Oceanogr.* **13**, 310-328 (1983).

Baker, L. E., Mashayek, A. & Naveira Garabato, A. C. Boundary upwelling of Antarctic Bottom Water by topographic turbulence. *AGU Adv.* **4**, e2022av000858 (2023).

Bluteau, C. E., Jones, N. L. & Ivey, G. N. Turbulent mixing efficiency at an energetic ocean site. *J. Geophys. Res.* **118**, 4662-4672 (2013).

de Lavergne, C., Madec, G., Le Sommer, J., Nurser, A. J. G. & Naveira Garabato, A. C. On the consumption of Antarctic Bottom Water in the abyssal ocean. *J. Phys. Oceanogr.* **46**, 635-661 (2016).

de Lavergne, C., Groeskamp, S., Zika, J. & Johnson, H. The role of mixing in the large-scale ocean circulation. In *Ocean Mixing: Drivers, Mechanisms and Impacts*, M. P. Meredith & A. C. Naveira Garabato (Eds.), Elsevier (2021).

Drake, H. F., Ferrari, R. & Callies, J. Abyssal circulation driven by near-boundary mixing: Water mass transformations and interior stratification. *J. Phys. Oceanogr.* **50**, 2203-2226 (2020).

Ferrari, R., Mashayek, A., McDougall, T. J., Nikurashin, M. & Campin, J.-M. Turning ocean mixing upside down. *J. Phys. Oceanogr.* **46**, 2239-2261 (2016).

Garrett, C. Comment on 'Some evidence for boundary mixing in the deep ocean' by L. Armi. *J. Geophys. Res.* **84**, 5095 (1979).

Gregg, M. C., D'Asaro, E. A., Riley, J. J. & Kunze, E. Mixing efficiency in the ocean. *Ann. Rev. Mar. Sci.* **10**, 443-473 (2018).

Grimshaw, R. H. J., Baines, P. G. & Bell, R. C. The reflection and diffraction of internal waves from the junction of a slit and a half-space, with application to submarine canyons. *Dyn. Atmos. Oce.* **9**, 85-120 (1985).

Harris, P. T. & Whiteway, T. Global distribution of large submarine canyons: Geomorphic differences between active and passive continental margins. *Mar. Geol.* **285**, 69-86 (2011).

Harris, P., Macmillan-Lawler, M., Rupp, J. & Baker, E. Geomorphology of the oceans. *Mar. Geol.* **352**, 4-24 (2014).

Holliday, N. P. *et al.* Multidecadal variability of potential temperature, salinity, and transport in the eastern subpolar North Atlantic. *J. Geophys. Res.* **120**, 5945-5967 (2015).

Ivey, G. N., Bluteau, C. E., Gayen, B., Jones, N. L. & Sohail, T. Roles of shear and convection in driving mixing in the ocean. *Geophys. Res. Lett.* **48**, e2020gl089455 (2021).

Klymak, J. M., Pinkel, R., Liu, C.-T., Liu, A. K. & David, L. Prototypical solitons in the South China Sea. *Geophys. Res. Lett.* **33**, L11607 (2006).

Kunze, E. Internal-wave-driven mixing: Global geography and budgets. *J. Phys. Oceanogr.* **47**, 1325-1345 (2017a).

Kunze, E. The internal-wave-driven meridional overturning circulation. *J. Phys. Oceanogr.* **47**, 2673-2689 (2017b).

Lewin, S. F. & Caulfield, C. P. Stratified turbulent mixing in oscillating shear flows. *J. Fluid Mech.*

944, R3 (2022).

Liu, C.-L., Kaminski, A. K. & Smyth, W. D. The effects of boundary proximity on Kelvin-Helmholtz instability and turbulence. *J. Fluid Mech.* **966**, A2 (2023).

Lorke, A., Peeters, F. & Wüest, A. Shear-induced convective mixing in bottom boundary layers on slopes. *Limn. Oceanogr.* **50**, 1612-1619 (2005).

Lorke, A., Umlauf, L. & Mohrholz, V. Stratification and mixing on sloping boundaries. *Geophys. Res Lett.* **35**, L14610 (2008).

Lumpkin, R. & Speer, K. Global ocean meridional overturning. *J. Phys. Oceanogr.* **37**, 2550-2562 (2007).

Ma, Y., Ferrari, R., Polzin, K., Alford, M., Naveira Garabato, A. & Voet, G. Standing wave-induced tidal shear in a submarine canyon in the Rockall Trough. *J. Phys. Oceanogr.*, submitted (2025).

MacKinnon, J. *et al.* Climate Process Team on internal wave-driven ocean mixing. *Bull. Am. Met. Soc.* **98**, 2429-2454 (2017).

Masunaga, E., Alford, M. H. & Bellerjeau, C. Mechanisms of internal tide-induced turbulent mixing observed from mooring data in a shallow steep submarine canyon. J. Phys. Oceanogr., in press (2025).

Melet, A., Hallberg, R. & Marshall, D. P. The role of ocean mixing in the climate system. In *Ocean Mixing: Drivers, Mechanisms and Impacts*, M. P. Meredith & A. C. Naveira Garabato (Eds.), Elsevier (2021).

Moum, J., Perlin, A., Klymak, J. M., Levine, M. D., Boyd, T. & Kosro, P. M. Convectively driven mixing in the bottom boundary layer. *J. Phys. Oceanogr.* **34**, 2189-2202 (2004).

Munk, W. Abyssal recipes. *Deep-Sea Res.* **13**, 707-730 (1966).

Munk, W. & Wunsch, C. Abyssal recipes II: Energetics of tidal and wind mixing. *Deep-Sea Res. I* **45**, 1977-2010 (1998).

Nazarian, R. H. & Legg. S. Internal wave scattering in continental slope canyons, part 1: Theory

443 and development of a ray tracing algorithm. *Ocean Model.* **118**, 1-15 (2017a).

444 Nazarian, R. H. & Legg. S. Internal wave scattering in continental slope canyons, part 2: A
445 comparison of ray tracing and numerical simulations. *Ocean Model.* **118**, 16-30 (2017b).

446 Nazarian, R. H., Burns, C. M., Legg, S., Buijsman, M. C., Kaur, H. & Arbic, B. K. On the magnitude
447 of canyon-induced mixing. *J. Geophys. Res.* **126**, e2021jc017671 (2021).

448 Oakey, N. S. Determination of the rate of dissipation of turbulent energy from simultaneous
449 temperature and velocity shear microstructure measurements. *J. Phys. Oceanogr.* **12**, 256-
450 271 (1982).

451 Polzin, K. L. & McDougall, T. J. Mixing at the ocean's bottom boundary. In *Ocean Mixing:*
452 *Drivers, Mechanisms and Impacts*, M. P. Meredith & A. C. Naveira Garabato (Eds.), Elsevier
453 (2021).

454 Sarkar, S. & Scotti, A. From topographic internal gravity waves to turbulence. *Ann. Rev. Fluid*
455 *Mech.* **49**, 195-220 (2017).

456 Schulz, K. & Umlauf, L. Residual transport of suspended material by tidal straining near sloping
457 topography. *J. Phys. Oceanogr.* **46**, 2083-2102 (2016).

458 Shaw, W. J., Trowbridge, J. H. & Williams III, A. J. Budgets of turbulent kinetic energy and scalar
459 variance in the continental shelf bottom boundary layer. *J. Geophys. Res.* **106**, 9551-9564
460 (2001).

461 Si, Y., Ferrari, R. & Ma, Y. Tidally-driven turbulence in the deep ocean. *Proc. Nat. Acad. Sci.*,
462 submitted.

463 Slinn, D. N. & Riley, J. J. Turbulent mixing in the oceanic boundary layer caused by internal wave
464 reflection from sloping terrain. *Dyn. Atmos. Oc.* **24**, 51-62.

465 Smyth, W. D. & Moum, J. N. Ocean mixing by Kelvin-Helmholtz instability. *Oceanogr.* **25**, 140-
466 149 (2012).

467 Sreenivasan, K. R. Turbulent mixing: A perspective. *Proc. Nat. Acad. Sci.* **116**, 18175-18183
468 (2018).

Stanev, E. V. & Ricker, M. Interactions between barotropic tides and mesoscale processes in deep ocean and shelf regions. *Ocean. Dyn.* **70**, 713-728 (2020).

Talley, L. D. Closure of the global overturning circulation through the Indian, Pacific, and Southern Oceans: Schematics and transports. *Oceanogr.* **26**, 80-97 (2013).

Thorpe, S. A. The turbulent ocean. Cambridge University Press (2005).

Umlauf, L. & Burchard, H. Diapycnal transport and mixing efficiency in stratified boundary layers near sloping topography*. J. Phys. Oceanogr.* **41**, 329-345 (2011).

Waterhouse, A. F. *et al.* Global patterns of diapycnal mixing from measurements of the turbulent dissipation rate. *J. Phys. Oceanogr.* **44**, 1854-1872 (2014).

Whalen, C. B. *et al.* Internal wave-driven mixing: governing processes and consequences for climate. *Nature Rev. Earth Env.* **1**, 606-621 (2020).

Winters, K. B. Tidally driven mixing and dissipation in the stratified boundary layer above steep submarine topography. *Geophys. Res Lett.* **42**, 7123-7130 (2015).

Winters, K. B. & D'Asaro, E. A. Diascalar flux and the rate of fluid mixing. *J. Fluid Mech.* **317**, 179-193 (1996).

Wynne-Cattanach, B. *et al.* Observations of diapycnal upwelling within a sloping submarine canyon. *Nature* **630**, 884-890 (2024).

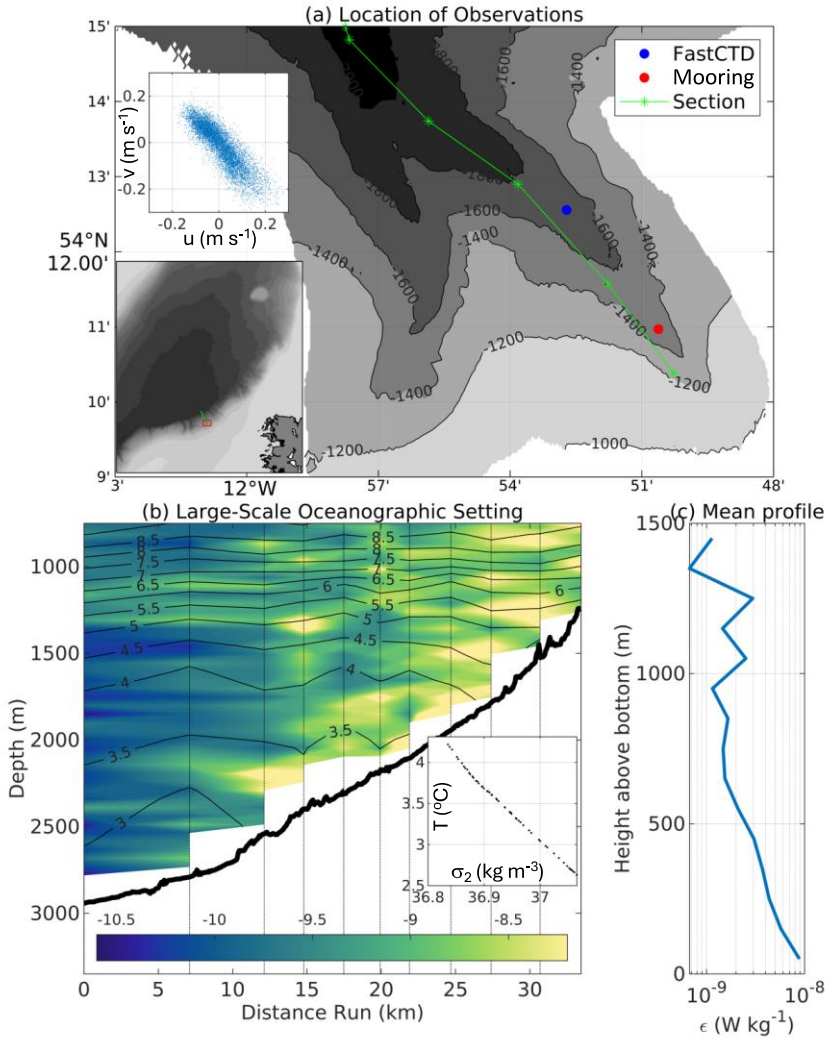

Figure 1 | Overview of BLT-Recipes experimental domain and observations. (a) Topography of the Rockall Trough in the Northeast Atlantic (lower inset), and of the continental-slope canyon measured during the BLT-Recipes experiment (main panel) with measurement locations indicated by instrument-referencing symbols. The near-bottom (averaged over a height above bottom range of 50-300 m) velocity at the location of the mooring is shown in the upper inset, and indicates that tidal fluctuations in the in-canyon flow are predominantly oriented along the canyon. (b) Logarithm of the rate of turbulent kinetic energy dissipation (ε, shading) and potential temperature (contours) along the canyon's thalweg (section marked in Fig. 1a). The inset illustrates the potential temperature (*T*) - density relationship observed within the canyon, where the density variable shown (σ_2) is the potential density relative to 2000 dbar. (c) Along-canyon-mean profile of ε versus height above bottom.

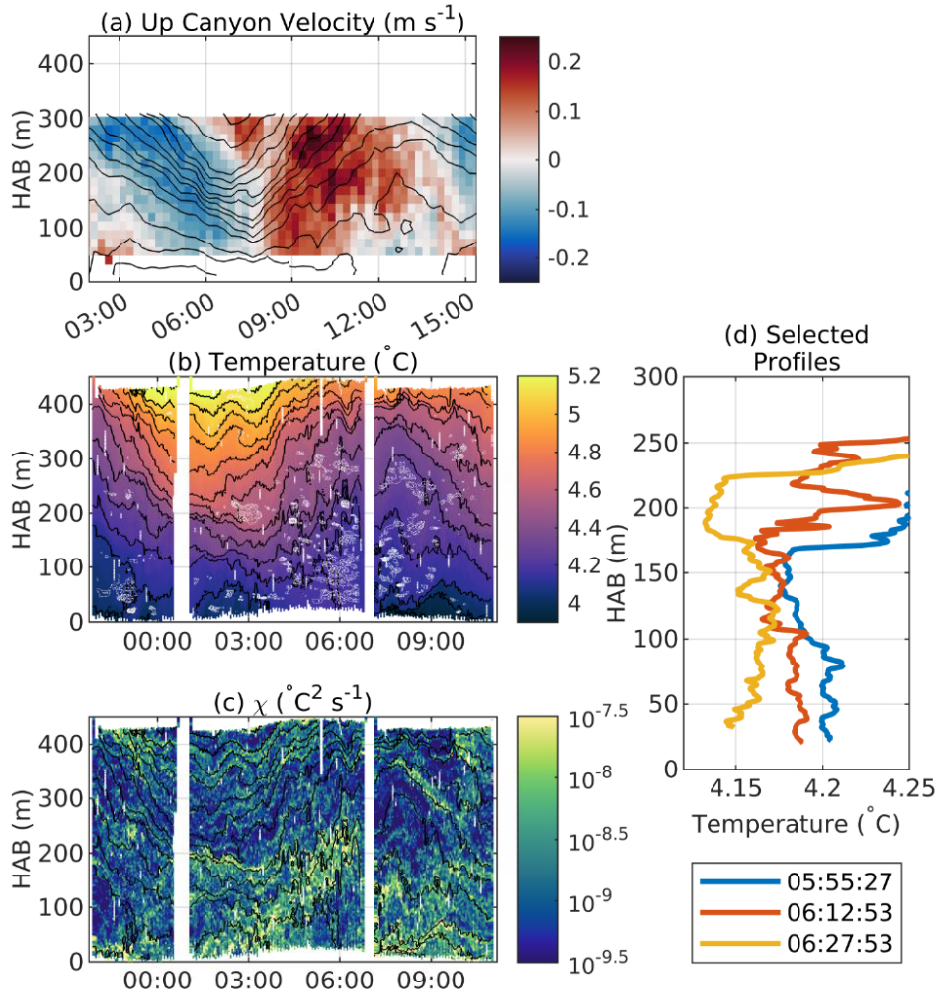

Figure 2 | A semidiurnal tidal cycle of along-canyon flow, hydrographic structure and turbulent mixing. (a) Along-canyon velocity (shading, positive values indicate up-canyon flow) and potential temperature (contours) measured by the mooring's ADCP and thermistors, respectively, on 8 July 2021. HAB: height above bottom. (b) Potential temperature (shading and black contours) measured by the FastCTD on 2-3 July 2021. White contours indicate occurrences of a statically unstable vertical temperature gradient (i.e. $\partial T/\partial z < 0$). (c) Rate of turbulent dissipation of temperature variance (χ, shading) measured by the FastCTD, with potential temperature contours overlaid in black. Panels (a) and (b)-(c), which show data from different periods at approximately the same location, have been aligned by the phase of the semidiurnal tide. (d) Selected profiles of potential temperature during the period with extensive statically unstable conditions.

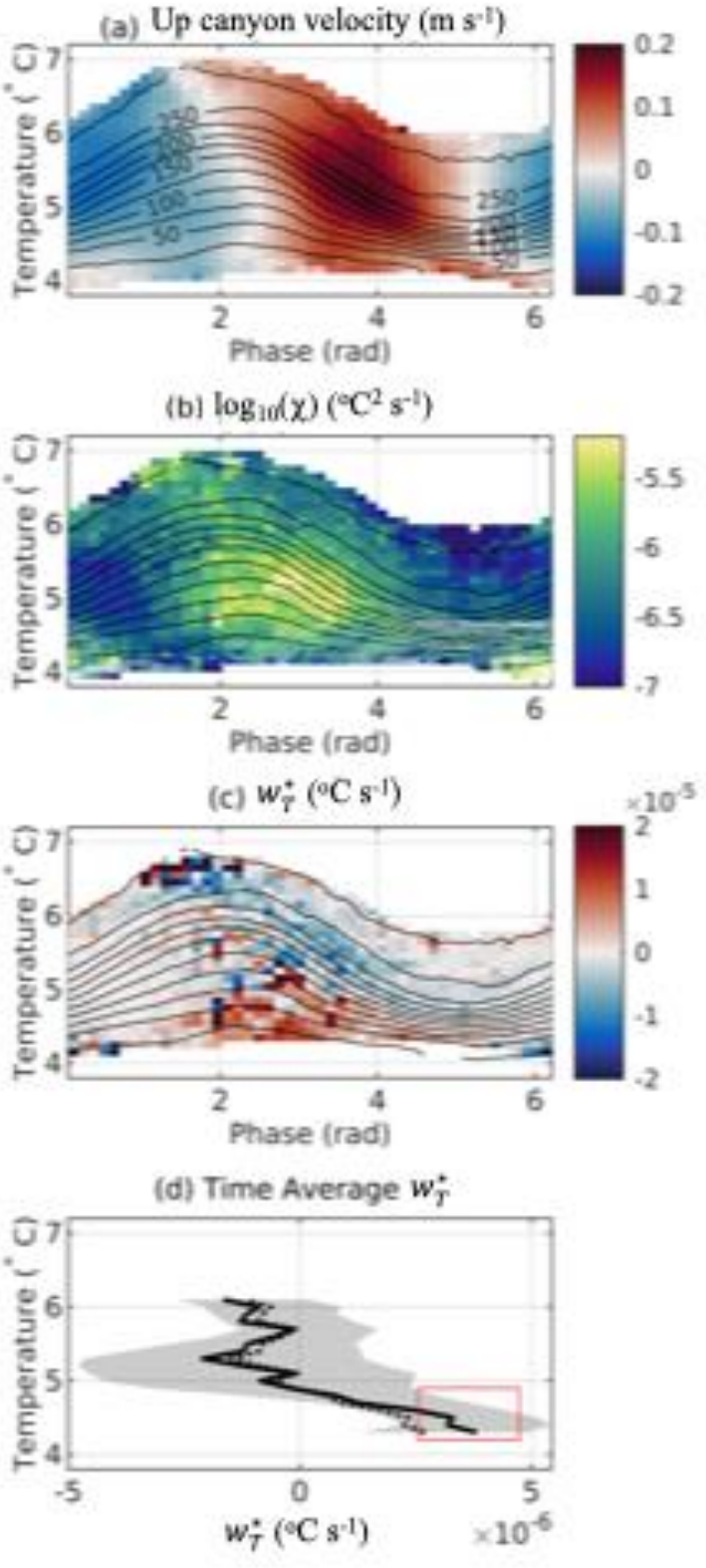

Figure 3 | Phase-averaged semidiurnal tidal cycle of along-canyon flow, turbulent mixing and diapycnal upwelling. Phase-averaged (a) up-canyon velocity, (b) rate of turbulent dissipation of

513 temperature variance (χ), and (c) diapycnal velocity (w_T^*) – indicated by shading in each panel –
514 as a function of potential temperature for a characteristic semidiurnal tidal cycle. Height above
515 bottom contours are overlaid in black and labelled in (a). (d) Mean (across all phases) profile of
516 diapycnal velocity as a function of potential temperature. The solid and dashed lines
517 respectively show the diapycnal velocity calculated using dissipation ratio (Γ) values of 0.2 and
518 0.4 (see Suppl. Info.). The grey shading provides a measure of the uncertainty in w_T^* related to
519 temporal variability and instrumental noise. This is computed as the interquartile range of w_T^*
520 estimates obtained from many phased-averaged χ fields, each constructed from a set of three
521 semidiurnal tidal periods. The diapycnal velocity determined from the dye (Wynne-Cattanach et
522 al., 2024) is added as a rectangle (with horizontal and vertical side lengths respectively
523 indicating the uncertainty and the potential temperature range sampled by the dye, where this
524 range has been shifted toward warmer waters by the difference between the coldest
525 temperatures sampled by the dye and the mooring) for comparison.
526

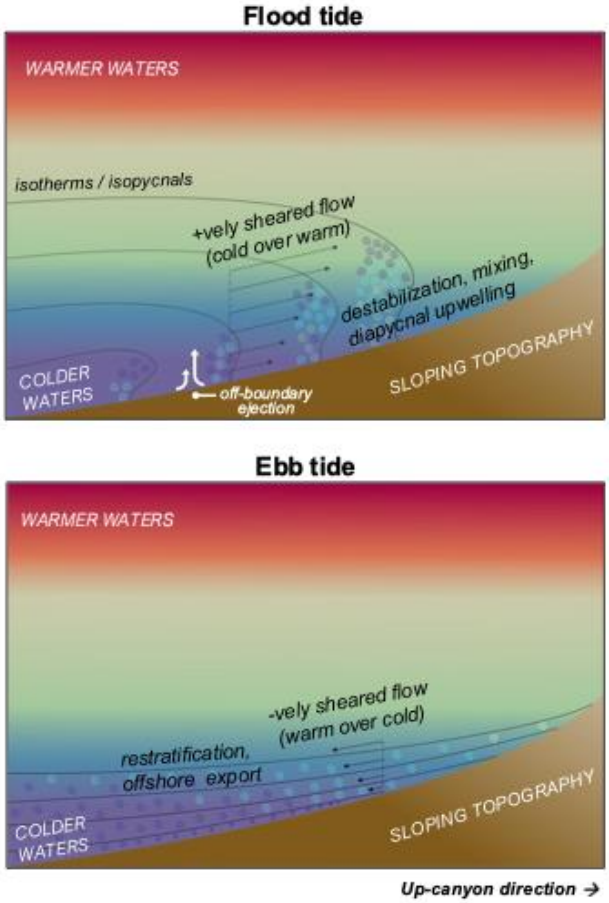

527

528 **Figure 4 | Schematic of along-boundary upwelling driven by tidally-generated convective**
529 **mixing.** (a) During flood tide, the positively sheared up-canyon flow (black arrows) causes
530 relatively dense waters aloft to overshoot, reducing stratification and producing mixing with
531 lighter waters – thus leading to diapycnal upwelling of the dense waters along the boundary. (b)
532 During ebb tide, the intensification of down-canyon flow with height (negatively sheared flow,
533 shown by black arrows) induces re-stratification within the canyon, and supports the offshore
534 export of waters that were newly mixed and upwelled during the previous flood tide. The small
535 circular swirls in both panels denote turbulent eddies, shaded by temperature / density.

Geophysical Research Letters

Supporting Information for

Connecting Mixing to Upwelling along the Ocean's Sloping Boundary

Alberto C. Naveira Garabato[1], Carl P. Spingys[2], Bieito Fernández Castro[1], Nicole Couto[3], Henri F. Drake[4], Alexander Forryan[1], Zhiyuan Gao[1,5], Yuchen Ma[6], Herlé Mercier[7], Marie-José Messias[8], Xiaozhou Ruan[9], Gunnar Voet[3], Bethan L. Wynne-Cattanach[3], Raffaele Ferrari[6], Matthew H. Alford[3] and Kurt L. Polzin[10]

[1]Ocean and Earth Science, University of Southampton, Southampton, SO14 3ZH, UK.

[2]National Oceanography Centre, Southampton, SO14 3ZH, UK.

[3]Scripps Institution of Oceanography, University of California San Diego, La Jollxa, CA 92037, USA.

[4]Department of Earth System Science, University of California Irvine, Irvine, CA92697-3100, USA.

[5]Key Laboratory of Physical Oceanography, Ocean University of China, Qingdao, 266100, China

[6]Department of Earth, Atmospheric and Planetary Sciences, Massachusetts Institute of Technology, Cambridge, MA 02139, USA.

[7]Laboratoire de Physique des Océans, CNRS, UMR 6523 CNRS / Ifremer / IRD / UBO, Ifremer Centre de Brest, Plouzané, France.

[8]College of Life and Environmental Sciences, University of Exeter, Exeter, EX4 4QE, UK.

[9]Department of Earth and Environment, Boston University, Boston, MA 02215, USA.

[10]Woods Hole Oceanographic Institution, Woods Hole, MA 02543, USA.

Contents of this file:

Introduction

This file provides:

- A detailed description of the dataset used in this work.
- An account of the processing of shear and temperature microstructure data
- A description of the methodology to calculate turbulent mixing rates from mooring-based temperature observations
- An exploratory discussion of the relative roles of convective and shear instabilities in driving mixing
- An account of the methodology to compute phase-averaged fields
- A description of the uncertainty in the calculation of diapycnal upwelling rates
- An exploratory discussion of the origin of the along-canyon shear
- Supplementary figures to illustrate the above
- A supplementary movie of the mooring record of along-canyon flow, hydrography and turbulent mixing

Text S1.

Experimental design

A set of targeted, vessel-based measurements of the hydrographic, velocity and (shear and temperature) microstructure properties of the ocean within and above a continental-slope canyon in the Rockall Trough (Northeast Atlantic; Fig. 1a) was acquired during expedition DY132 of the *RRS Discovery* between 19th June and 29th July 2021, supported by the U.K.-U.S. Bottom Boundary Layer Turbulence and Abyssal Recipes (BLT-Recipes) programme. See Figure 1 for a map overview of the measurements pertinent to this article.

These ship-based observations were collected with two instrument suites. First, the general along-canyon distributions of stratification and mixing were documented with a transect of 11 full-depth stations along the canyon's thalweg. At each station, vertical profiles (down to 5-50 m above the ocean floor) of hydrographic variables and velocity were recorded with: (i) a conductivity-temperature-depth / 300-kHz lower acoustic Doppler current profiler (CTD/LADCP) package lowered from the vessel; and (ii) the untethered, free-fall Woods Hole Oceanographic Institution's High Resolution Profiler (HRP) (Polzin and Montgomery, 1996) or Rockland Scientific Vertical Microstructure Profiler 6000 (VMP-6000) (Naveira Garabato et al., 2016), which additionally measured shear and temperature microstructure – from which the rates of dissipation of turbulent kinetic energy (ε) and temperature variance (χ) can be respectively quantified (Oakey, 1982). Second, 6 finely-resolved (with a characteristic temporal resolution of ~15 min) time series of hydrographic and temperature microstructure profiles spanning 1-2 semidiurnal tidal cycles were obtained within the canyon, over a height-above-bottom range of approximately 0-400 m, using two Scripps Institution of Oceanography-produced, lightly-tethered ultra-fast profilers equipped with a CTD and either conductivity (from which temperature was derived) microstructure sensors (the FastCTD) or shear and temperature microstructure sensors (the Epsilometer) (Le Boyer et al., 2021). The FastCTD, which was also integrated with a fluorometer, enabled monitoring of the dispersion of a fluorescein dye injected near the seabed, from which evidence of very rapid diapycnal upwelling along the canyon is drawn and discussed by Wynne-Cattanach et al. (2024). All microstructure profilers produced processed data with a vertical resolution of 0.5 m. Full details of the dataset acquisition and processing may be found in the DY132 cruise report (Naveira Garabato and Spingys, 2021).

Vessel-based measurements were supplemented by moored observations of turbulent fluctuations in three-component velocity and temperature, obtained with a mooring instrumented with 7 modular acoustic velocity sensor (MAVS) current meters (not explicitly considered here), 83 fast-sampling thermistors and an ADCP. The mooring was deployed near the canyon's head (Fig. 1a) on 7th July 2021, during the DY132 expedition, and recovered on 4th October 2021 in cruise DY138 of the *RRS Discovery*. The fast-sampling thermistors were placed at intervals of 1-5 m (with higher vertical resolution near the seabed) over the

height-above-bottom range of 2-300 m, and were programmed to sample at 1 Hz over a period of 89 days. A downward-looking 75 kHz RDI ADCP was deployed in a float at the top of the mooring, at a height above bottom of 300 m, and sampled with a vertical bin size of 16 m every 15 minutes. Thus, the moored measurements were performed at a substantially finer temporal resolution, and during a much longer period – extending over ~172 semidiurnal tidal cycles and ~106 inertial cycles – than the ship-based observations. As such, the moored sensors sampled the variability in turbulent parameters, and its relationships with the evolving background stratification and flow, with far greater statistical robustness than provided by the vessel-based data.

Calculation of turbulent kinetic energy dissipation rates from shear microstructure measurements

The rate of dissipation of turbulent kinetic energy, ε, was computed from shear microstructure measurements obtained with three different profilers (HRP, VMP-6000 and Epsilometer; see *Experimental design*), which recorded vertical gradients in horizontal velocity on centimetre scales at 512 Hz to within typically 2 m of the ocean floor. Data processing was conducted using algorithms developed originally for the HRP (Polzin and Montgomery, 1996; Naveira Garabato et al., 2016; Le Boyer et al., 2021; Naveira Garabato and Spingys, 2021), which comply with current best practices (Lueck et al., 2024). The variance in the shear in the vertical direction, $\overline{(\partial u/\partial z)^2}$, was calculated every 0.5 m, using shear spectra computed over bin widths of 1 s and integrated between 1 Hz and the spectral minimum in the 10–25 Hz band, or the 25–100 Hz band for $\varepsilon > 10^{-7}$ W kg^{-1}. Values of ε were calculated from the variance of the shear as $\varepsilon = 7.5\,\nu\overline{(\partial u/\partial z)^2}$, where ν is the molecular viscosity of seawater and isotropy is assumed (Oakey, 1982).

Calculation of turbulent mixing rates from temperature microstructure measurements

The rate of dissipation of temperature variance, χ, was computed from temperature microstructure measurements acquired with four different profilers (HRP, VMP-6000, FastCTD and Epsilometer; see *Experimental design*). Similarly to ε, data processing was conducted using algorithms developed originally for the HRP (Polzin and Montgomery, 1996; Naveira Garabato et al., 2016; Le Boyer et al., 2021; Naveira Garabato and Spingys, 2021). The variance of the vertical temperature gradient, $\overline{(\partial T/\partial z)^2}$, was calculated every 0.5 m, using bin widths of 1 s. Each profiler carried two fast-response thermistors, and unless one sensor was deemed noisy, the mean of the χ estimates from each sensor pair was used. Values of χ were computed from the variance of the vertical temperature gradient as $\chi = 6\kappa\overline{(\partial T/\partial z)^2}$, where κ the molecular diffusivity of seawater and isotropy is assumed (Oakey, 1982). Prior to the computation of χ, $\overline{(\partial T/\partial z)^2}$ was corrected for nonlinearity and pressure dependence in the thermistors' response by reference to the temperature measurements obtained with a CTD mounted on each profiler. Microstructure cast locations were recorded as the midpoint between the instrument deployment and recovery positions in each station (HRP and VMP-6000), or as the vessel's position at the time of sampling (FastCTD and EpsiFish).

Fundamentally, χ represents the rate of dissipation of temperature variance by molecular mixing. Since this temperature variance is produced by centimetre-scale turbulent diathermal motions acting on the evolving temperature field, χ provides a metric of the diathermal mixing effected by such motions (Winters and D'Asaro, 1996). In the context of our canyon data set, the diathermal and diapycnal directions are closely aligned, as evidenced by the tightness of the in-canyon potential temperature-density relationship (Fig. 1b). This relationship is quasi-linear and monotonic, with an R^2 value of 0.996 and a linear-fit root-mean-square error of 0.004 kg m^{-3}. Thus, χ adequately quantifies the intensity of turbulent diapycnal mixing within the canyon.

Calculation of turbulent mixing rates from mooring-based temperature observations

The rate of dissipation of temperature variance, χ, was computed from temperature time series acquired with each of the 83 fast-sampling (1 Hz) thermistors in the mooring. χ can be estimated from temperature records by fitting a theoretical model of inertial subrange turbulence to measured temperature spectra (Shaw et al., 2001; Bluteau et al., 2013; Sreenivasan, 2018),

$$\phi_T(k) = C_\theta \chi \varepsilon^{-\frac{1}{3}} k^{-\frac{5}{3}} \quad , \qquad \text{(S1)}$$

where $\phi_T(k)$ is the horizontal wavenumber spectrum of temperature, k is the horizontal wavenumber, and C_θ is the Obukhov-Corrsin constant (taken as 0.4). This wavenumber inertial subrange spectral model is translated to frequency, σ, via Taylor's frozen field hypothesis, $\sigma = Uk$, with U as the magnitude of the flow past the sensor (Shaw et al., 2001; Bluteau et al., 2013). Relating the rate of dissipation of turbulent kinetic energy, ε, to a buoyancy flux (Shaw et al., 2001), and assuming the buoyancy frequency to be a function of temperature only, then yields:

$$\chi = \left[\left(\frac{g\alpha}{2\Gamma \frac{\partial \overline{T}}{\partial z^*}} \right)^{\frac{1}{3}} \left(\frac{2\pi}{U} \right)^{\frac{2}{3}} \sigma^{-\frac{5}{3}} \frac{\phi_T(\sigma)}{C_\theta} \right]^{\frac{3}{2}}, \qquad \text{(S2)}$$

where g is gravity, α is the thermal expansion coefficient, and Γ is the dissipation ratio (the ratio of the net change in potential energy due to turbulent mixing to the energy expended in producing the turbulence; Gregg et al., 2018). This expression enables χ to be calculated from theoretical fits to the observed temperature spectra. In our implementation, we computed spectra in 5-minute segments, scaled them by $\sigma^{5/3}$, and averaged the (fitted and scaled) spectra for periods of 10-100 s (or 10-[hab/U] s for instruments whose height above bottom (hab) was sufficiently small that hab/U < 100 s) representative of the inertial subrange. This produced an estimate of χ every 5 minutes for each thermistor. Γ was taken as 0.2 (a common value in much of the ocean; Gregg et al., 2018), but the sensitivity of χ to this choice was explored by repeating the calculation with Γ = 0.4 (a value that is likely more appropriate to our measured canyon; Alford et al., 2025).

A number of practical computation choices must be made in estimating χ from thermistor measurements, including: the window size and shape implemented in the Welch spectral calculation; the frequency range used to average the temperature spectra; the application of the mean or median operators in averaging over this frequency range; and the aforementioned selection of a Γ value. We performed a broad suite of sensitivity tests using a representative sample of the entire thermistor data set, in order to assess the robustness of our χ estimates. The resulting χ data were only weakly sensitive to reasonable variations in computation choices. Thus, changes in spectral window size (between 20 s and 300 s) and shape (Hamming vs. Hann windows), and in mean vs. median operator choice, produced a change in χ of at most a factor of 1.7. Similarly, χ exhibited weak sensitivity to the choice of frequency range for spectral averaging (upper and lower bounds varied from 10^{-2} Hz to 0.2 Hz): χ values changed by less than a factor of 1.5, except when excessive narrowness of the frequency range increased the impact of spectral noise. Varying Γ from 0.2 to 0.4 resulted in a reduction in χ by a factor of 1.4. We also conducted a thorough examination of 5-min-averaged temperature spectra for each thermistor to ensure that the selected frequency range is representative of the inertial subrange, with spectra consistently exhibiting the typical -5/3 (i.e. -1.67) slope (median slopes averaged for each instrument vary from -2.19 to -1.48, with a standard deviation of 0.34). Finally, we probed the influence of replacing the bin-averaged ADCP measurements of U by data from point current meters (MAVS), where available, on χ; such influence proved to be minimal (less than a factor of 1.5).

Assessment of the physics leading to the onset of turbulence and mixing

Turbulent diapycnal mixing in the stratified ocean interior is commonly associated with shear-driven turbulence (Thomas and Zhai, 2021; Musgrave et al., 2021; Mashayek et al., 2021). Such turbulence ensues when a stably stratified fluid with buoyancy frequency $N = \sqrt{-(g/\rho)(\partial\rho/\partial z)}$ (with ρ as density) and subjected to a steady flow with vertical shear $S = \partial U/\partial z$ (with U as flow speed) becomes unstable to shear instability, which grows as the gradient Richardson number $Ri = N^2/S^2 < 0.25$ (Miles, 1961; Howard, 1961;

Thorpe, 2005; Ivey et al., 2021). The Ri criterion becomes less strict when the vertical shear is unsteady (Kelly, 1965; Radko, 2019; Si et al., 2025) or there is pre-existing turbulence in the fluid (Kaminski and Smyth, 2019). In the presence of strong shears, like that reported in the canyon, dense waters can also be advected over lighter waters and trigger a convective instability, with progressive mixing of the unstable patch from above (Moum et al., 2004; Lorke et al., 2005, 2008; Umlauf and Burchard, 2011; Winters, 2015; Ivey et al., 2021).

To quantitatively assess which instability may trigger the vigorous mixing ($\chi > 10^{-8}$ °C^2 s^{-1}) observed once per tidal cycle, we develop a simple two-dimensional (along-canyon distance versus depth) analytical model to explore how the in-canyon potential temperature distribution, which characterizes the in-canyon stratification, is affected by the observed along-canyon flow over a typical semidiurnal tidal cycle. The in-canyon temperature field is assumed to depend solely on depth, $T(x,z) = T(z)$ (with x representing the along-canyon distance), meaning that mean isotherms are taken as approximately flat within the canyon in line with our measurements (Fig. 1b), and is initialised from mooring observations at the time of ebb-to-flood tide reversal. The horizontal component of the along-canyon flow u is approximated as a function of height above the local bottom (hab) and time (t), i.e. $u(x,z,t) = u(hab(x),t)$, with the flow's vertical component assumed to be vertically uniform within the canyon and parallel to the canyon's thalweg, i.e. $w(x,t) = \eta\, u(x,z,t)$, where $\eta \approx 0.07$ is the bottom slope of the canyon's thalweg. These approximations assume that (i) the along-canyon velocity profile measured by the mooring is widely representative along the canyon's thalweg, and (ii) the component of the flow normal to the seafloor plays a modest role in the advection of temperature within the canyon. Some support for (i) is provided by the recurrent pattern of isothermal displacement and χ over a semidiurnal tidal cycle observed at various locations along the canyon (e.g., compare Figures 2 and S2, constructed from measurements acquired 5 km apart). Regarding (ii), the moored observations of along-canyon and vertical velocity (Fig. S5) show that particle trajectories are up to 40% steeper than the canyon's thalweg during flood tide, indicating that our model assesses only instabilities associated with the slope-parallel shear flow, and so neglects instabilities caused by the additional uplift of isopycnals by the flow component perpendicular to the seafloor. Assumption (ii) effectively neglects the potential influence of nonlinear internal wave deformation and breaking in triggering mixing (Slinn and Riley, 1996; Winters, 2015; Cyr and van Haren, 2016).

The model is integrated in time over a semidiurnal (flood followed by ebb) period and an effectively unbounded along-canyon domain, in order to estimate the depth from which waters sampled by the mooring at each time originated (Fig. S1). A model integration for the same period as shown in Figure 2a is considered here – other periods yield very similar results. During the flood phase of the tide, water parcels translate a characteristic up-canyon distance of ~2.5 km at ~250 m above the seafloor but only <1 km within ~80 m of the seafloor, i.e. waters aloft move up-canyon by >1.5 km relative to near-bottom waters (not shown). With along-canyon parcel trajectories assumed parallel to the sloping seafloor, the differential up-canyon motion

of waters with a substantial height above bottom relative to those below causes waters arriving at the mooring's deepest ~250 m during flood tide to originate from a narrow range of depth (and therefore temperature) horizons (Fig. S1). Such homogenization of deep water properties generates a weakly stratified BBL at the time of strong shear, creating the conditions for instabilities to grow. This suggestion is reaffirmed by the favourable comparison of the model's predictions with the observed temperature record (Fig. S1), which indicates that the measured emergence of a thick, homogeneous BBL during flood tide stems from all BBL waters having been sourced over a narrow range of depths upstream.

The specific nature of the instability, however, remains unclear. Si et al. (2025) find that even when the stratification is at its minimum, the large-scale tidal shear is not sufficiently strong to bring Ri below 0.25. Instead, they propose that the tidal flow goes unstable to a parametric instability associated with the time dependence of the tidal shear, which can arise at the $Ri \sim 1$ observed in the canyon. Alford et al. (2025) rather suggest that finite-amplitude perturbations to the low-mode tidal shear associated with topographic roughness or propagating internal waves can generate fluid patches with $Ri < 0.25$, thereby seeding the development of the instability. Polzin (in preparation) emphasizes that the enhancement of tidal shear near the seafloor by bottom drag is another potential pathway to instability, consistent with the evidence that turbulent mixing originates from the seafloor and propagates upward. In conclusion, there is no shortage of explanations for why instability and mixing develop when the stratification is reduced in the canyon. The specific pathway does not really matter for the present work. The key point here is that instability and mixing are triggered by the tidal shear acting on the background stratification within the canyon, with the vertical scale of the well-mixed BBL being set by that of the tidal shear (see *Origin of the along-canyon shear*).

Constructing a phase-averaged view of a semidiurnal tidal cycle

To draw statistically robust relationships between mixing and its tidal drivers, and elucidate implications for upwelling, we construct a phase-averaged picture of the temporal evolution of the along-canyon flow (Fig. 3a), χ (Fig. 3b) and a range of ancillary parameters (Fig. S5) over a semidiurnal tidal cycle. The time series of phase used to generate the averages is calculated by fitting a sinusoid to the up-canyon velocity over a sliding 3-day window. This sinusoid has four free parameters (amplitude, frequency, phase and offset) that are separately fitted via a least squares approach for each window. The resulting fitted phase is then taken as the phase at the mid-point of the window. This approach was employed to capture possible subtle changes in the tidal drivers over the time series. An analogous analysis using a fixed M2 period produces very similar phase-averaged diagnostics, although slightly blurred due to smoothing by small phase errors.

Uncertainty in the calculation of diapycnal upwelling from mooring-based temperature observations

To gauge the uncertainty in w_T^* related to temporal variability and instrumental noise, we compute the interquartile range of w_T^* estimates obtained from many phased-averaged χ fields, each constructed from a

set of three semidiurnal tidal periods (the smallest record length required to map out χ as a function of potential temperature and tidal phase) (Fig. 3d). This suggests that, at a minimum, the near-boundary upwelling signal of w_T^* in waters colder than ~5°C is robust and persistent during the period of mooring observations. Although errors in the thermistor-based estimates of χ (discussed in *Calculation of turbulent mixing rates from mooring-based temperature observations*) may potentially introduce further quantitative uncertainty in w_T^*, such errors are too modest to affect our conclusions on near-boundary upwelling.

Origin of the along-canyon shear

The along-canyon shear exerts an important influence on the intensity of upwelling within the canyon, as it is this shear that triggers turbulent overturns by differentially advecting denser waters over lighter waters during flood tide and resetting a stable stratification during the ebb phase (Fig. S1). To gain some insight into the along-canyon shear's physical origin, Figure S4a shows the power density frequency spectrum of the ADCP-measured along-canyon velocity shear, estimated from a linear fit to the full vertical profile of the along-canyon velocity. The spectrum exhibits peaks at the K1 and M2 tidal frequencies and their harmonics, with little energy at the higher frequencies related to small-scale turbulence. Further, the along-canyon shear is much more energetic than the cross-canyon shear (not shown). This confirms that the shear is associated with along-canyon baroclinic tidal motions within the canyon.

Next, we wish to assess whether the tidal shear results from turbulent motions arresting the near-bottom flow – as might be expected from the action of topographic drag – or from the propagation of waves (e.g., baroclinic tides) within the canyon. To illuminate this issue, Figure S4b displays the coherence between the along-canyon and vertical velocities, which provides a metric of the effectiveness of motions of a given frequency in the vertical redistribution of along-canyon momentum. Such redistribution is arguably required to explain the emergence of the tidal shear. Coherence is found to be large exclusively at tidal frequencies, and not at the higher frequencies of small-scale turbulent flows. This strongly suggests that the tidal shear is associated with baroclinic waves that arise in the canyon (Baines, 1983; Grimshaw et al., 1985; Ma et al., 2025), and not the result of a turbulent-frequency momentum flux divergence. The observed dominance of the shear's along-canyon component further suggests that the waves' dispersion relationship is Kelvin-like (Rhines, 1970), in that cross-canyon motions are suppressed by the presence of supercritical lateral walls. Future work will address the question of how these waves are generated.

Although the ADCP measurements used in this analysis do not resolve the full spectrum of small-scale turbulent motions, the above results are corroborated through an analogous examination of MAVS current meter observations from the same mooring (not shown), which have much finer temporal resolution and comprehensively capture the inertial subrange.

Additional References (not contained in Main Text)

Cyr, F. & van Haren, H. Observations of small-scale secondary instabilities during the shoaling of internal bores on a deep-ocean slope. *J. Phys. Oceanogr.* **46**, 219-231 (2016).

Howard, L. N. Note on a paper of John W. Miles. *J. Fluid Mech.* **10**, 509-512 (1961).

Howland, C. J., Taylor, J. R. & Caulfield, C. P. Testing linear marginal stability in stratified shear layers. *J. Fluid Mech.* **839**, R4 (2020).

Kaminski, A. & Smyth, W. Stratified shear instability in a field of pre-existing turbulence. *J. Fluid Mech.* **862**, 639-658 (2019).

Le Boyer, A., Alford, M. H., Couto, N., Goldin, M., Lastuka, S., Goheen, S., Nguyen, S., Lucas, A. J. & Hennon, T. D. Modular, flexible, low-cost microstructure measurements: the epsilometer. *J. Atmos. Ocean. Tech.* **38**, 657-668 (2021).

Lueck, R., Fer, I., Bluteau, C., Dengler, M., Holtermann, P., Inoue, R., Le Boyer, A., Nicholson, S.-A., Schulz, K. & Stevens, C. Best practices recommendations for estimating dissipation rates from shear probes. *Front. Mar. Sci.* **11**, 1334327.

Mashayek, A., Baker, L. E., Cael, B. B. & Caulfield, C. P. A marginal stability paradigm for shear-induced diapycnal turbulent mixing in the ocean. *Geophys. Res. Lett.* **49**, e2021gl095715 (2021).

Miles, J. W. On the stability of heterogeneous shear flows. *J. Fluid Mech.* **10**, 496-508 (1961).

Musgrave, R., Pollmann, F., Kelly, S. & Nikurashin, M. The lifecycle of topographically-generated internal waves. In *Ocean Mixing: Drivers, Mechanisms and Impacts*, M. P. Meredith & A. C. Naveira Garabato (Eds.), Elsevier (2021).

Naveira Garabato, A. C., Polzin, K. L., Ferrari, R., Zika, J. D. & Forryan, A. A microscale view of mixing and overturning across the Antarctic Circumpolar Current. *J. Phys. Oceanogr.* **46**, 233-254 (2016).

Naveira Garabato, A. C. & Spingys, C. Bottom Boundary Layer Turbulence and Abyssal Recipes (BLT-Recipes), National Oceanography Centre Southampton Cruise Report, https://www.bodc.ac.uk/resources/inventories/cruise_inventory/reports/dy132.pdf (2021).

Polzin, K. L. & Montgomery, E. T. Deep microstructure profiling with the High Resolution Profiler. *Proc. Microstructure Sensors Workshop*, Mt. Hood, OR, Office of Naval Research, 109-115 (1996).

Polzin, K. L., Wang, B., Wang, Z., Thwaites, F. & Williams III, A. J. Moored flux and dissipation estimates from the northern Deepwater Gulf of Mexico. *Fluids* **6**, 237 (2021).

Radko, T. Instabilities of a time-dependent shear flow. *J. Phys. Oceanogr.* **49**, 2377-2392 (2019).

Rhines, P. Edge-, bottom- and Rossby waves in a rotating stratified fluid. *Geophys. Astrophys. Fluid Dyn.* **1**, 273-302 (1970).

Thomas, L. N. & Zhai, X. The lifecycle of surface-generated near-inertial waves. In *Ocean Mixing: Drivers, Mechanisms and Impacts*, M. P. Meredith & A. C. Naveira Garabato (Eds.), Elsevier (2021).

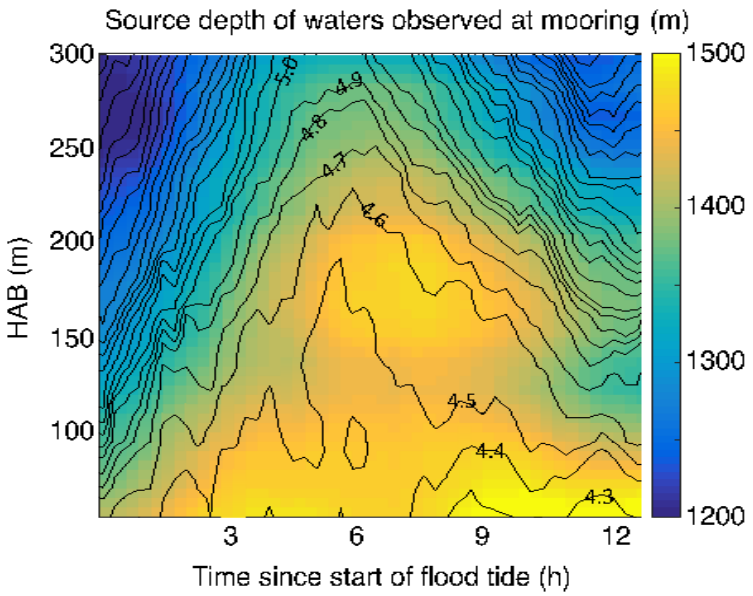

Figure S1 | Analytical model of the role of vertically differential along-canyon advection in generating reduced stratification. Source depth (shading) of waters sampled by the mooring, estimated with an idealized analytical model of the advection of the in-canyon vertical temperature profile at the start of flood tide by the measured along-canyon flow. Comparison with the observed potential temperature record (contours) indicates that the measured emergence of a thick, homogeneous BBL in the deepest ~250 m during flood tide stems from all BBL waters having originated at approximately the same depth upstream, thus priming the layer for convective or shear instabilities. Conversely, BBL thinning coincides with a progressive sharpening of the vertical gradient in the source depth of near-bottom waters. HAB: height above bottom.

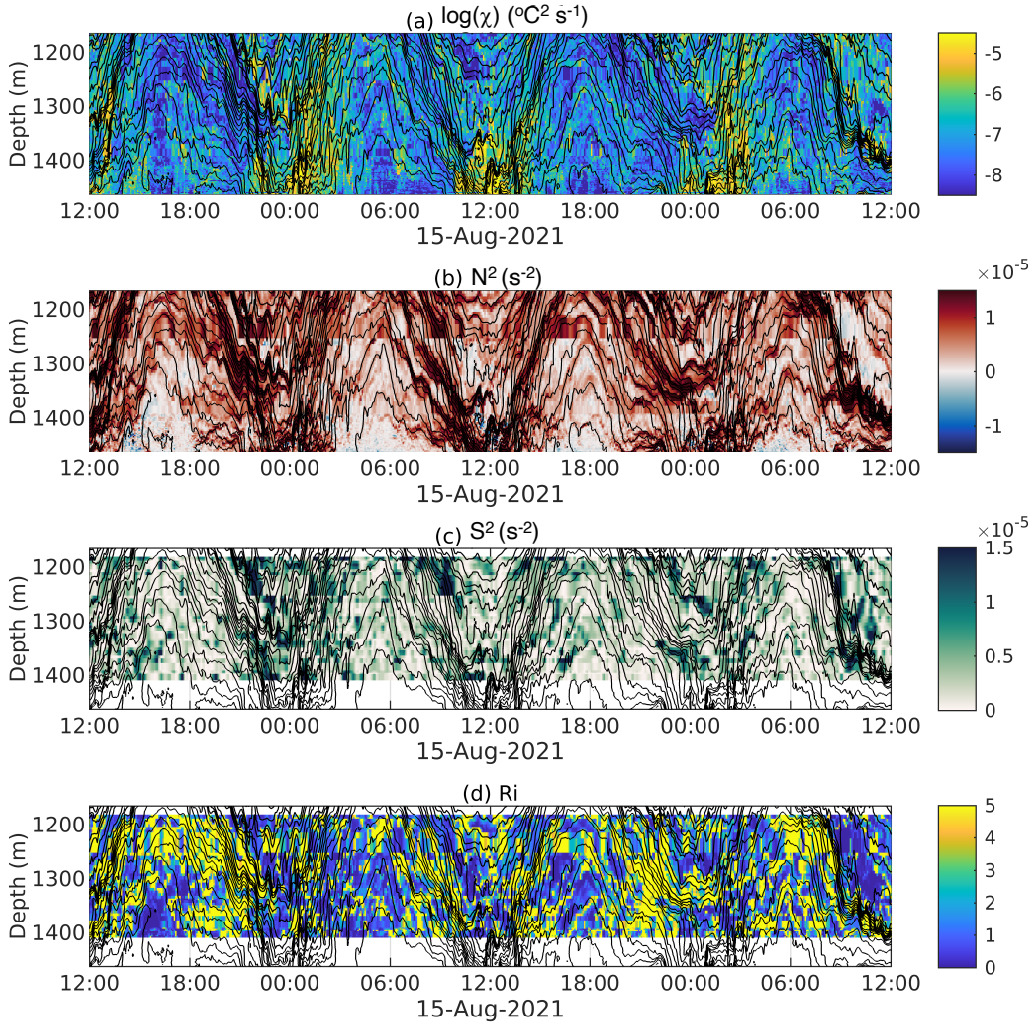

Figure S2 | A 2-day example of semidiurnal cycles of turbulent mixing, in-canyon stratification, shear and Richardson number. (a) Rate of turbulent dissipation of temperature variance (χ, shading) and potential temperature (contours) during a 2-day subset of the mooring record. (b) Squared buoyancy frequency (N^2, shading) and potential temperature (contours) during the same period. (c) Squared shear (S^2, shading) and potential temperature (contours). (d) Richardson number (Ri, shading) and potential temperature (contours).

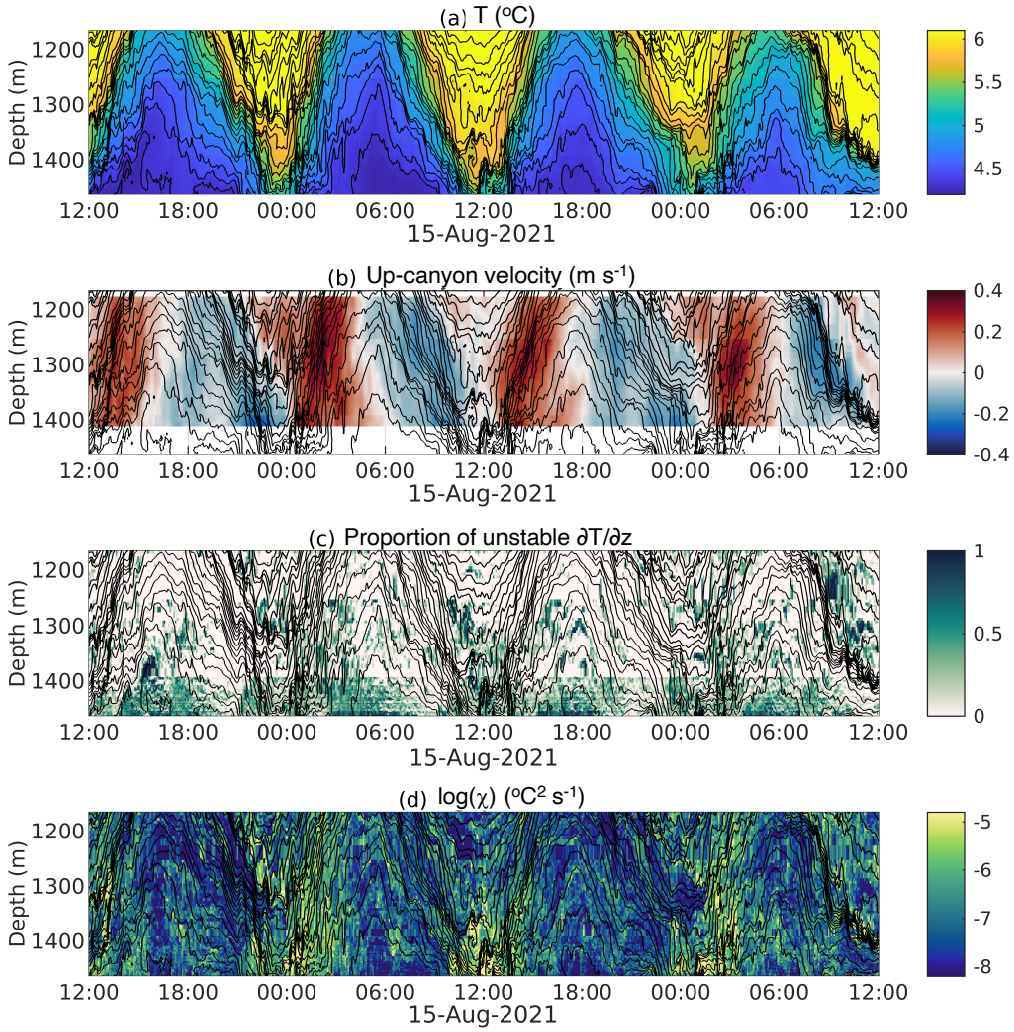

Figure S3 | A 2-day example of semidiurnal cycles of hydrographic structure, along-canyon flow and turbulent mixing. (a) Potential temperature (shading and black contours) during a 2-day subset of the mooring record. (b) Along-canyon velocity (shading) and potential temperature (contours) in the same period. (c) Fractional occurrence of a statically unstable vertical temperature gradient (i.e. $\partial T/\partial z < 0$) in the 1 Hz temperature data within each 15-min bin (shading), with potential temperature contours overlaid in black. A fraction of 1 indicates sustained unstable conditions within a bin, and a fraction of 0 denotes continuous stability during that time. (d) Rate of turbulent dissipation of temperature variance (χ, shading) and potential temperature (contours).

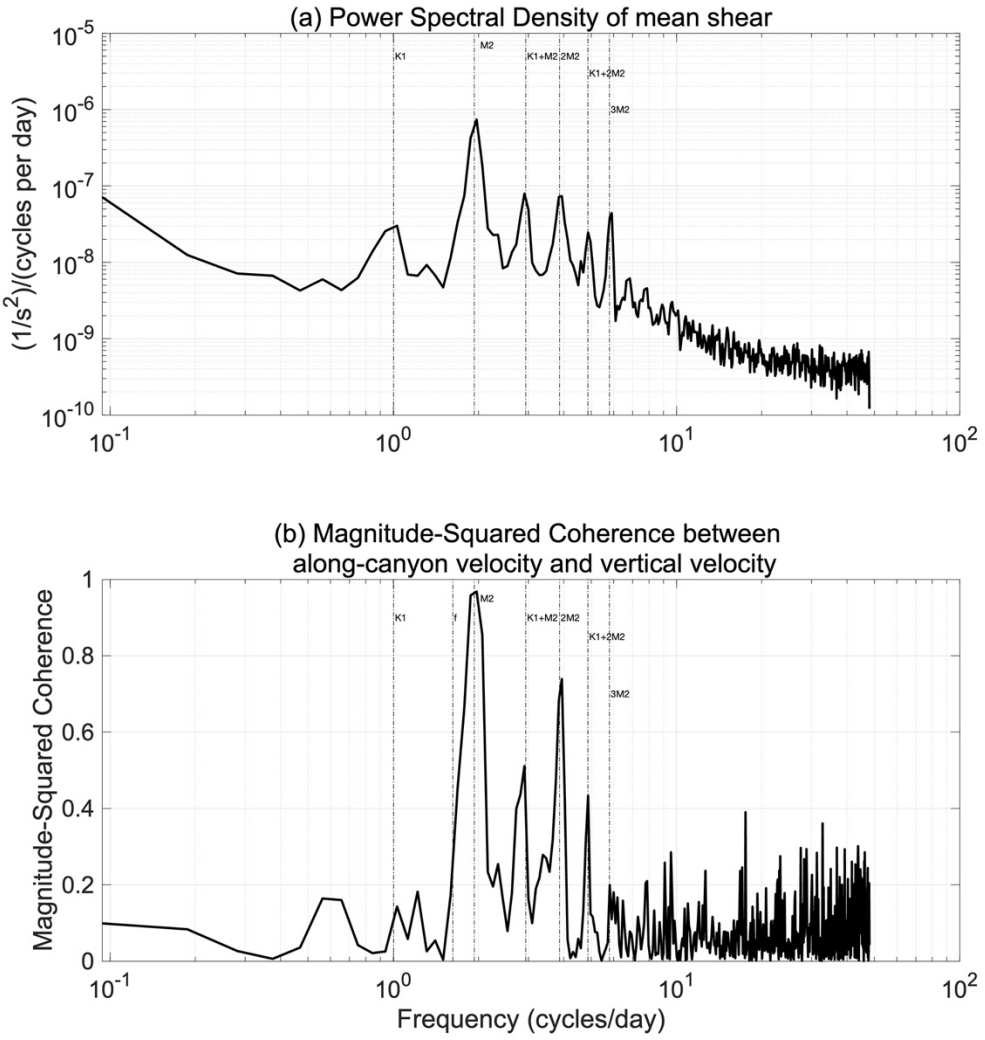

Figure S4 | Investigation of the physical origin of along-canyon shear. (a) Power spectral density of the (ADCP-measured) mean along-canyon velocity shear, estimated from a linear fit to the full vertical profile of the along-canyon velocity. (b) Magnitude-squared coherence between the along-canyon velocity and the vertical velocity. The K1 and M2 tidal constituents and their harmonics are indicated by dashed lines and labelled in both panels.

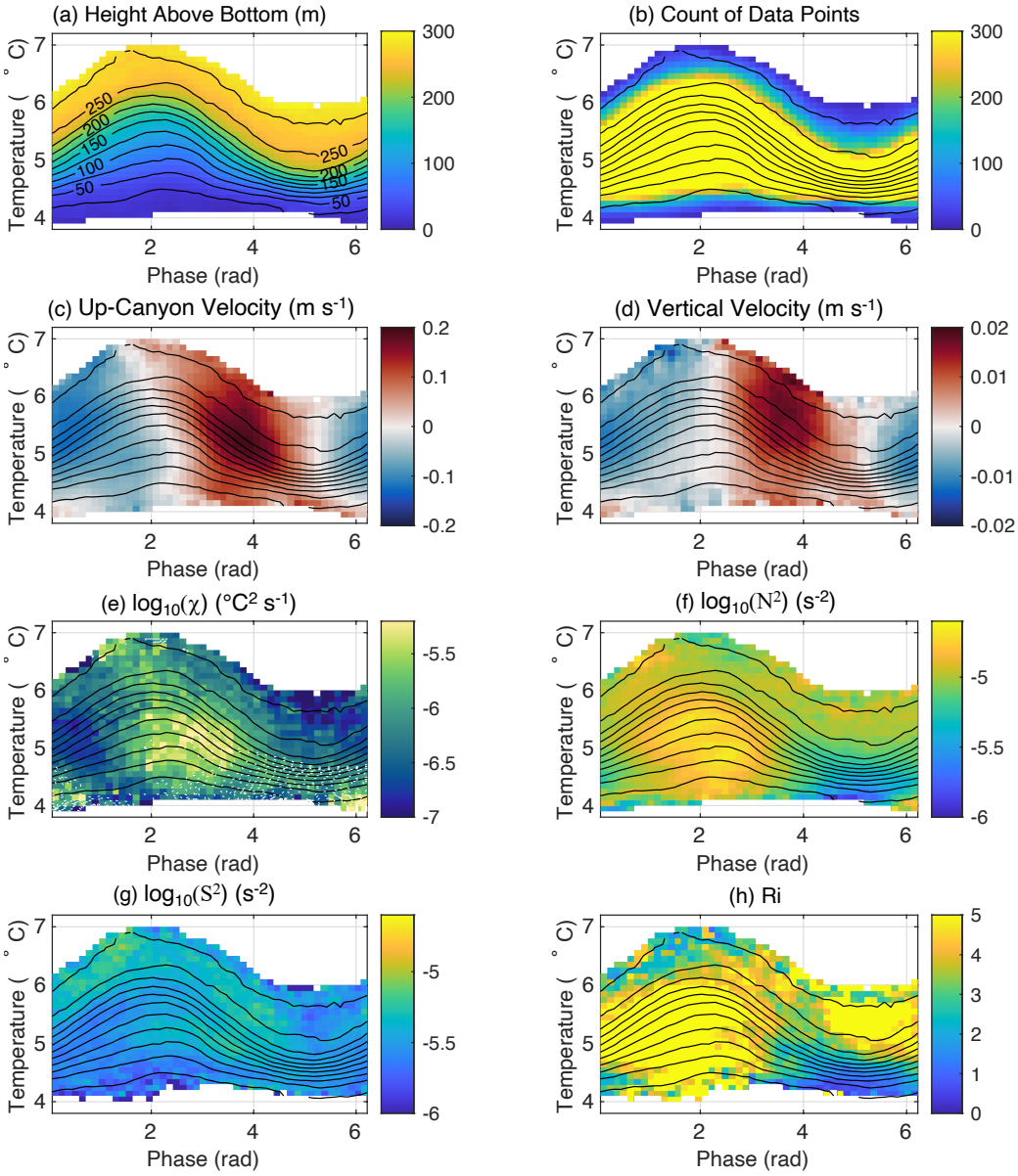

Figure S5 | Phase-averaged semidiurnal tidal cycle of in-canyon flow, hydrographic structure and turbulence parameters. Phase-averaged (a) height above bottom of isotherms; (b) data density; (c) up-canyon velocity; (d) vertical velocity; (e) rate of dissipation of temperature variance (χ); (f) squared buoyancy frequency (N^2); (g) squared shear (S^2); and (h) Richardson number (Ri) – as a function of potential temperature for a characteristic semidiurnal tidal cycle (shading). Height above bottom contours are overlaid in black and labelled.

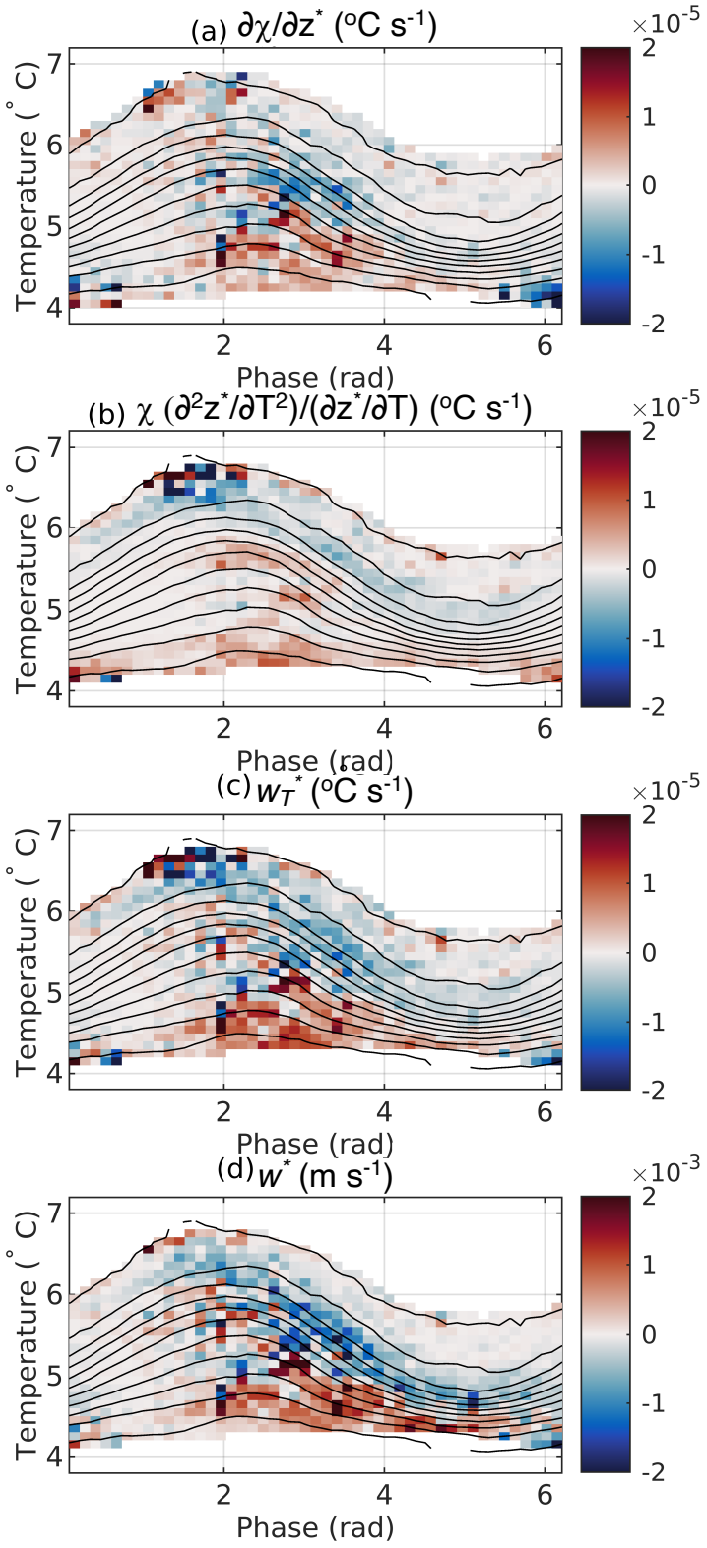

Figure S6 | Phase-averaged semidiurnal tidal cycle of diapycnal upwelling and its constituent terms. Phase-averaged (a) $\frac{\partial \chi}{\partial T}$ term of diapycnal velocity, (b) $\chi \frac{\partial^2 z^*/\partial T^2}{\partial z^*/\partial T}$ term of diapycnal velocity, (c) diapycnal velocity expressed as a warming rate (w_T^*), and (d) diapycnal velocity in m s^{-1} ($w^* \approx w_T^* / \frac{\partial T}{\partial z}$) – indicated by shading

in each panel – as a function of potential temperature for a characteristic semidiurnal tidal cycle. Height above bottom contours are overlaid in black.

Movie S1 | An 89-day mooring record of along-canyon flow, hydrographic structure and turbulent mixing. (a) Up-canyon velocity (shading) and potential temperature (contours) during the 89-day mooring record. (b) Potential temperature (shading and contours) in the same period. (c) Rate of turbulent dissipation of temperature variance (χ, shading, on a logarithmic scale), with potential temperature contours overlaid in black.

https://www.dropbox.com/scl/fi/s8284vnyiq511r8i0fup8/output.mp4?rlkey=4mxovtglqu1x2eouaqhxx5fql&dl=0